

# Laser-Nucleus Interactions: The Quasiadiabatic Regime

Adriana Pálffy,<sup>1,\*</sup> Oliver Buss,<sup>2</sup> Axel Hoefer,<sup>3</sup> and Hans A. Weidenmüller<sup>1,†</sup>

<sup>1</sup>Max-Planck-Institut für Kernphysik, Saupfercheckweg 1, D-69117 Heidelberg, Germany

<sup>2</sup>AREVA GmbH, Dept. Radiology & Criticality, Kaiserleistr. 29, D-63067 Offenbach am Main, Germany

<sup>3</sup>AREVA GmbH, PEPAI-G Radiology & Criticality, Kaiserleistr. 29, D-63067 Offenbach am Main, Germany  
(Dated: December 7, 2024)

The interaction between nuclei and a strong zeptosecond laser pulse with coherent MeV photons is investigated theoretically. We provide a first semi-quantitative study of the quasiadiabatic regime where the photon absorption rate is comparable to the nuclear equilibration rate. In that regime, multiple photon absorption leads to the formation of a compound nucleus in the so-far unexplored regime of excitation energies several hundred MeV above the yrast line. The temporal dynamics of the process is investigated by means of a set of master equations that account for dipole absorption, stimulated dipole emission, neutron decay and induced fission in a chain of nuclei. That set is solved numerically by means of state-of-the-art matrix exponential methods also used in nuclear fuel burnup and radioactivity transport calculations. Our quantitative estimates predict the excitation path and range of nuclei reached by neutron decay and provide relevant information for the layout of future experiments.

PACS numbers: 25.20.-x, 24.60.Dr, 25.70.Gh, 42.50.Ct, 21.10.Pc

Keywords:

## I. INTRODUCTION

Recent experimental developments in laser physics promise to open the new field of laser-induced nuclear reactions in a domain of excitation energies that has not been explored so far. Efforts are under way [1] to generate a multi-MeV zeptosecond pulsed laser beam at the Nuclear Physics Pillar of the Extreme Light Infrastructure (ELI) now under construction in Romania [2] and at the International Center on Zetta-Exawatt Science and Technology (IZEST) [3]. Furthermore, theoretical proposals for the generation of coherent gamma-ray frequency combs at ELI have also been put forward [4]. How will an intense laser pulse interact with a medium-weight or heavy target nucleus? The nucleus is a strongly bound system. Therefore, the laser-nucleus interaction is weak in comparison to the laser-atom one. A reaction that differs significantly from the standard photon-induced nuclear reaction is expected to occur only if the photons in the laser pulse are coherent. Only then does the effective dipole width attain values in the MeV range, making it comparable with other characteristic nuclear energy scales. In this paper we accordingly consider the interaction of a strong coherent zeptosecond laser pulse with a medium-weight or heavy nucleus with mass number  $A$ . The pulse contains  $N = 10^3 - 10^4$  coherent photons, the energy  $E_L$  per photon is several MeV, and the duration of the pulse is  $\hbar/\sigma$  where  $\sigma$  is of the order of several 10 keV so that  $\hbar/\sigma \approx 10^{-20}$  s. Relevant questions then are: (i) How does the interaction of that laser pulse differ from laser-matter interaction in other areas of physics [5]? (ii) Which are the reactions that we expect to occur? The answers are obviously interesting in their own right and relevant for the layout of future experiments.

In the present paper we provide a partial answer to these questions by addressing the quasiadiabatic regime of the laser-nucleus interaction. In that regime, the process of photon absorption and that of nuclear relaxation are governed by similar time scales. The paper follows the study of the perturbative regime by one of the authors [6] where the absorption process is much slower than nuclear relaxation. We hope to be able to address the sudden regime (characterized by the converse situation) in a future paper. A brief summary of first qualitative results for the quasiadiabatic regime has been published in Ref. [7].

Our approach is based on the master equation describing the excitation and relaxation of the nucleus under the influence of the external field provided by the laser. Multiple absorption of coherent photons leads to nuclear excitation far above yrast. Setting up the master equation requires, therefore, the knowledge of the  $A$ -particle level density  $\rho_A$  at high excitation energies and for large particle numbers  $A$ , expressed in terms of the single-particle level density  $\rho_1$ . That is a challenging problem because near its maximum and for  $A \gtrsim 100$ ,  $\rho_A$  is several ten orders of magnitude bigger than  $\rho_1$ . An important preparatory step in our work has been the construction of a reliable approximation for  $\rho_A$  in terms of  $\rho_1$  [8, 9].

Use of the master equation renders possible the semiquantitative study of the competition between photon absorption, stimulated photon emission, photon-induced nucleon emission, neutron evaporation, and induced fission. In the absence of particle emission and fission, photon absorption would saturate at an excitation energy where the widths for absorption and for stimulated emission become equal. That is the case at the energy where the level density  $\rho_A$  reaches its maximum. Neutron evaporation takes over at an energy below the saturation point. The combination of repeated neutron emission and continued dipole absorption by the daughter nuclei then produces proton-rich nuclei far from the valley of stability. Although the induced fission width is small in comparison to all other widths, fission eventually terminates the reaction chain unless

\*Electronic address: palfy@mpi-hd.mpg.de

†Electronic address: haw@mpi-hd.mpg.de

the laser pulse comes to an end beforehand. In the latter case, laser-nucleus interaction experiments promise to shed light on nuclei at excitation energies far above yrast and far from stability.

A qualitative description of the expected processes and a definition of the quasiadiabatic regime are given in Sec. II. The master equation and the transition rates are introduced in Sec. III. This section also contains a semiquantitative estimate of the energies and time scales involved in the photon-absorption, neutron-evaporation and fission processes. Numerical results follow in Sec. IV and the paper concludes with a discussion in Sec. V.

## II. GENERAL CONSIDERATIONS

Nuclei are bound by the strong interaction. As a consequence, even the interaction of the strong laser pulse defined in the Introduction with a nucleus is much less violent than the interaction of a medium-intensity optical laser pulse with an atom. We substantiate that statement with the help of the Keldysh parameter [10]  $\gamma = \sqrt{2mI\omega}/(e\mathcal{E})$  used in atomic physics. Here,  $m$  and  $e$  are mass and charge of the electron, respectively,  $I$  is the field-free ionization potential, and  $\omega$  and  $\mathcal{E}$  are the frequency and electric field strength, respectively, of the laser pulse. The Keldysh parameter determines the dominant interaction mechanism in atoms. For  $\gamma < 1$  tunneling ionization dominates while for  $\gamma \gg 1$  the process is governed by multiphoton ionization. A small value of  $\gamma$  corresponds in the optical regime to an electric field strength  $\mathcal{E} \approx 10^9$  eV/cm of the laser. Such a field distorts the Coulomb potential of the atom so strongly that electrons are set free. The nuclear equivalent of the Keldysh parameter is obtained by replacing  $m$  by the nucleon mass ( $m \rightarrow 2000 m$ ),  $\omega$  by the photon energy ( $\omega \rightarrow 10^6 \omega$ ), and  $I$  by the binding energy of the last nucleon ( $I \rightarrow 10^7 I$ ). These substitutions increase the value of  $\gamma$  by a factor  $10^{11}$ . To return  $\gamma$  to a value less than unity, the field strength would have to increase by that same factor  $10^{11}$ , i.e.,  $\mathcal{E}$  would have to be of the order  $10^{20}$  eV/cm. This value roughly corresponds to the ratio of the binding energy of the last nucleon and the nuclear radius and, thus, to a distortion of the nuclear potential that roughly corresponds to the above-mentioned distortion of the Coulomb potential in atoms. In comparison with a standard laser, the photon energy in our laser pulse is increased by six orders of magnitude. Such an increase falls short by a wide margin of the necessary increase of  $\mathcal{E}$  by eleven orders of magnitude. Therefore, the laser-nucleus interaction is governed by a value  $\gamma \gg 1$  of the Keldysh parameter, and multiphoton processes dominate.

For photons in the MeV range, the product of photon wave number  $k$  and nuclear radius  $R$  obeys  $kR \ll 1$ . Therefore, we consider only dipole processes even though quadrupole excitation is important for some nuclei at small excitation energies [11]. For  $N \gg 1$  coherent photons in the laser pulse, dipole excitation is governed by the effective dipole width  $N\Gamma_{\text{dip}}$ . Here  $\Gamma_{\text{dip}}$  is the standard nuclear dipole width and is in the keV range. The amplification factor  $N$  applies in the semiclassical limit. For  $N\Gamma_{\text{dip}}$  we use values around 5 MeV.

Coherence is vital in bringing the effective dipole width up to values that are comparable with other characteristic nuclear energy scales defined below. Without coherence, the probability for the processes investigated in this paper would be dramatically reduced. In the course of the reaction, up to  $N_0 \approx 5 \times 10^2$  photons may be absorbed. We neglect the resulting reduction of  $N$  in the expression for  $N\Gamma_{\text{dip}}$ .

A further distinguishing feature of nuclei is that the nucleon-nucleon force is basically attractive, and that nuclei are self-bound. Nuclear properties are understood in terms of the shell-model potential (the mean field) plus the remaining “residual” nucleon-nucleon interaction. Because of the latter, distinct modes of nuclear excitation have the tendency to mix with the numerous other nuclear modes that are near the same excitation energy: the nucleus equilibrates. That property is absent in atoms. It qualitatively changes the treatment of the multistep photon absorption process. The time scale  $\hbar/\Gamma_{\text{sp}}$  for equilibration is expressed in terms of the spreading width  $\Gamma_{\text{sp}}$ , a manifestation of the residual interaction. The value of  $\Gamma_{\text{sp}}$  is known for low-lying modes with excitation energies of up to ten or twenty MeV where  $\Gamma_{\text{sp}}$  is of order  $\Gamma_{\text{sp}} \approx 5$  MeV [12].

The ratio  $N\Gamma_{\text{dip}}/\Gamma_{\text{sp}}$  relates the speed of dipole absorption with that of nuclear relaxation and, therefore, defines three regimes of the laser-nucleus interaction. (i) In the perturbative regime  $N\Gamma_{\text{dip}} \ll \Gamma_{\text{sp}}$ , single excitation of the collective dipole resonance in nuclei dominates. That regime has been investigated in Ref. [6]. Consequences for future experiments were theoretically explored in Ref. [13]. It was shown that if excited above neutron threshold, the time dependence of the nuclear decay is non-exponential, both in the neutron and in the gamma decay channels. (ii) In the sudden regime  $N\Gamma_{\text{dip}} \gg \Gamma_{\text{sp}}$  the residual nucleon-nucleon interaction is irrelevant. Nucleons are excited independently of each other and are emitted from the common average shell-model potential. The potential readjusts after nucleon emission. If the duration time  $\hbar/\sigma$  of the laser pulse is sufficiently large, the nucleus evaporates. The sudden regime is so far unexplored. (iii) The quasiadiabatic regime  $N\Gamma_{\text{dip}} \approx \Gamma_{\text{sp}}$  forms the topic of this paper. The nucleus (almost) attains statistical equilibrium between any two subsequent photon absorption processes.

A quasiadiabatic process occurs when the energy  $E_L$  per photon is less than or comparable with the nucleon binding energy  $E_B$  of around 8 MeV. Then absorption of a single photon does not lead to nucleon emission. Rather, the excitation energy is shared (almost) instantaneously with several or many other nucleons. The nucleus equilibrates. Another photon is absorbed, and the process repeats itself. Consecutive absorption of  $N_0 \gg 1$  photons leads to high excitation energies  $N_0 E_L$  of the (almost) equilibrated compound nucleus. The excitation process terminates either with the laser pulse or when all nuclei have fissioned. For the duration time  $\hbar/\sigma$  of the laser pulse, significant emission of particles sets in only after several or even many photons have been absorbed. Pre-compound reactions show that the condition  $E_L \leq E_B$  is not absolutely necessary [14]. If equilibration is sufficiently fast, a quasiadiabatic process will occur also for  $E_L > E_B$ .

With the nucleus close to equilibrium at all times, photon absorption leads to compound-nucleus formation at very high

energies. That situation is distinctly different from Coulomb excitation [18] or nuclear excitation by inelastic electron scattering [19]. In both these processes, modes of excitation very far from the equilibrated compound nucleus are formed at some excitation energy  $E$ . Such modes decay by particle emission and/or equilibration. If reached at all, the compound nucleus is formed at a much lower excitation energy than  $E$ .

The equilibration mechanism being absent in atoms, our theoretical description differs from the strong-field approximation in atomic physics [15, 16] and is related to the theory of precompound reactions [17]. As mentioned in the Introduction, we describe the process in terms of a set of time-dependent master equations. In addition to dipole absorption, we take stimulated dipole emission, neutron evaporation, and fission into account. Induced particle emission is briefly addressed in Section V.

We simplify the treatment in two respects. (i) We disregard spin altogether. (ii) We assume that after each photon absorption process, the nucleus attains full equilibrium. Both approximations simplify our treatment considerably. Without approximation (i), the number of master equations would be multiplied by the number of spin values considered. Without approximation (ii), the same would happen with regard to the number of configurations needed to describe equilibration at fixed excitation energy. While both approximations can easily be removed, the resulting increased complexity of the approach does not seem justified at this early stage of investigation and in view of the complete lack of experimental data.

To justify approximation (i), we calculate analytically in Appendix A the distribution of nuclear spin values after  $N_0$  photons have been absorbed by dipole transitions by a nucleus with ground state spin zero. This is done for  $N_0 \gg 1$ . The distribution peaks at spin  $J = \sqrt{N_0}$  and falls off very rapidly for larger values of  $J$ . Exact numerical results not based on the approximation  $N_0 \gg 1$  confirm this result, see Fig. 1. Even for a maximum number  $N_0 = 5 \times 10^2$  of absorbed photons, the nuclear spin does not significantly exceed 20 or so. This fact justifies our neglect of spin.

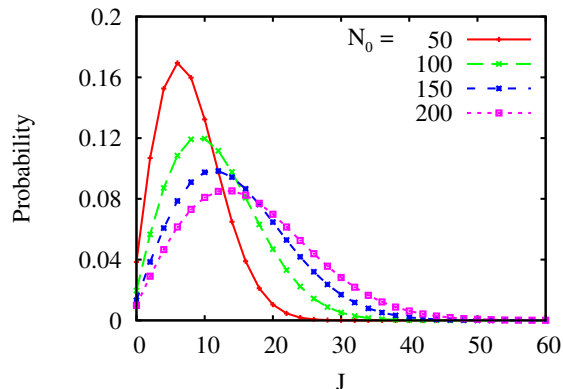


FIG. 1: (color online). Distribution of total spin values of the compound nucleus for several values of the number  $N_0$  of absorbed photons.

Approximation (ii) implies that in the master equation we

need not distinguish (as done in precompound reactions) the formation of  $n$ -particle  $n$ -hole states. Instead we work with the full set of equilibrated states at each excitation energy. To discuss the error made in approximation (ii), we observe that for a non-equilibrated system the mean number of  $n$ -particle  $n$ -hole pairs at fixed excitation energy is smaller than for the equilibrated system. That has two consequences. First, the number of states accessible for further dipole excitation is larger (because the exclusion principle blocks fewer states). Second, the mean excitation energy per particle or hole is larger, too. Therefore, neutron decay is more likely than in the equilibrated case (the number of available decay channels is increased). Both errors work in the same direction, leading within our approximation to an overestimate of the overall duration time of the excitation process. The resulting uncertainty can be compensated by varying the relative strength of photon excitation and neutron decay in the calculations.

### III. MASTER EQUATION

#### A. Basic Approach

With  $A$  the mass number of the target nucleus, we consider a chain of  $(n + 1)$  nuclei with mass numbers  $A - i$  where  $i = 0, 1, 2, \dots, n$ , with an arbitrary cutoff at  $i = n$ . In nuclei with even mass number  $A$ , the states with spin zero at excitation energy between  $(k - 1/2)E_L$  and  $(k + 1/2)E_L$  are grouped together and are jointly referred to as states  $(i, k)$ . Here  $E_L$  is the photon energy and  $k = 1, 2, \dots$ . The group of states with excitation energies in the interval  $0 \leq E \leq (1/2)E_L$  is labeled  $(i, 0)$ . The number of such states is determined by the level density  $\rho(A, E)$  of states with spin zero. For odd  $A$  we proceed analogously. For simplicity and in order to avoid the introduction of additional parameters we neglect the even-odd staggering of the ground-state energies as well as the spin-cutoff factor, and approximate the level density of spin  $1/2$  states by interpolating between the values for the two neighboring even  $A$  nuclei. In other words, we use the expression for  $\rho(A, E)$  valid for even  $A$  and given in Ref. [9] indiscriminately for both even and odd  $A$ . We construct the time-dependent master equation for the total occupation probability  $P(i, k, t)$  of these states as function of time  $t$ . The equation takes into account dipole excitation by the coherent laser pulse, stimulated dipole emission by the same pulse, both for every nucleus in the chain, and neutron decay populating nucleus  $A - i - 1$  at the expense of nucleus  $A - i$ . It is assumed that within each group  $k$  of states in nucleus  $A - i$ , the occupation probability is equilibrated at all times and, thus, proportional to the total level density  $\rho(i, k)$  for that group. That assumption is characteristic of the quasiadiabatic regime. Neglecting the emission of charged particles we confine ourselves to a chain of nuclei with equal proton numbers. Likewise we do not take account of particle loss due to direct photon excitation of particles into continuum states. We address the ensuing limitations and possible corrections below.

For the duration time  $1/\sigma$  of the laser pulse, the states  $(i, k)$  are fed by coherent dipole excitation of the states  $(i, k - 1)$  and

by stimulated dipole emission of the states  $(i, k+1)$ , and they are depleted by dipole absorption exciting the states  $(i, k+1)$  and by stimulated dipole emission to the states  $(i, k-1)$ . Using Fermi's golden rule we write the rates feeding the states  $(i, k)$  as  $W_{k'k}^2 \rho(i, k)$  with  $k' = k \pm 1$ . Here  $W_{k'k}^2 = W_{k'k}^2$  is the

square of the transition matrix element. Neutron decay depletes the states  $(i, k)$  at the rate  $\Gamma_N(i, k)$ . Neutron decay of the states  $(i-1, k')$  in the nucleus with mass number  $A+1-i$  feeds the states  $(i, k)$  with the rate  $\Gamma_N(i-1, k' \rightarrow k)$ . The master equation reads

$$\begin{aligned} \dot{P}(i, k, t) = & \Theta(1/\sigma - t) \left\{ \rho(i, k) [W_{kk-1}^2 P(i, k-1, t) + W_{kk+1}^2 P(i, k+1, t)] - P(i, k, t) [W_{kk-1}^2 \rho(i, k-1) + \right. \\ & \left. + W_{kk+1}^2 \rho(i, k+1)] \right\} + \sum_{k'} \Gamma_N(i-1, k' \rightarrow k) P(i-1, k', t) - \Gamma_N(i, k) P(i, k, t). \end{aligned} \quad (1)$$

Here,  $\hbar = 1$  and we have defined  $P(-1, k, t) = 0$ . The dot denotes the time derivative, and  $\Theta$  is the Heaviside function. The initial condition is  $P(i, k, 0) = \delta_{i0} \delta_{k0}$ . We require that neutron emission does not take place from the nucleus with mass number  $A-n$  and put  $\Gamma_N(n, k) = 0$  for all  $k$  so that nucleus  $(A-n)$  serves as a dump for the overall probability flow. For  $i = 0, 1, \dots, n-1$  we have

$$\Gamma_N(i, k) = \sum_{k'} \Gamma_N(i, k \rightarrow k'). \quad (2)$$

Then Eq. (1) implies  $\sum_{i,k} \dot{P}(i, k, t) = 0$ , and the master equation conserves total occupation probability.

Induced fission is taken into account by introducing a diagonal loss term  $-\Gamma_f(i, k) P(i, k, t)$  in Eq. (1). Here  $\Gamma_f(i, k)$  is the width for induced fission from state  $(i, k)$ . Fission leads to a depletion of the total occupation probability. We do not keep track of the fission products. Therefore, fission eventually terminates the laser-nucleus reaction. In the absence of induced fission and neutron decay (i.e., for  $\Gamma_N(i, k) = \Gamma_f(i, k) = 0$  for all  $(i, k)$ ), probability is conserved within the target nucleus,  $\sum_k \dot{P}(0, k, t) = 0$ . For  $\sigma \rightarrow 0$  (infinitely sharp laser energy with the laser pulse lasting forever) and  $\Gamma_N(i, k) = 0$  for all  $(i, k)$ , the target nucleus equilibrates, asymptotically ( $t \rightarrow \infty$ ) reaching the equilibrium distribution  $P_{\text{eq}}(0, k) \propto \rho(i, k)$  for all  $k$  values below and around the saturation energy.

## B. Transition Rates

The transition rates have been defined, calculated, and discussed in Ref. [7]. We present these rates here for the sake of completeness. Because of the approximations explained below in the calculation of the level density, particular values of the transition rates might differ from the ones presented in Ref. [7]. Since  $\hbar = 1$  we use the expressions “width” and “rate” interchangeably.

### 1. Dipole Transitions

With  $\Gamma_{\text{dip}}$  the standard nuclear dipole absorption width and  $N$  the number of coherent photons in the laser pulse, the effective dipole width for the ground state is given by  $N\Gamma_{\text{dip}}$ . That expression holds for  $N \gg 1$  in the semiclassical approximation. With  $\Gamma_{\text{dip}}$  in the keV range and  $N \approx 10^3$  or  $10^4$ , the effective dipole width is of the order of several MeV. The value of  $N\Gamma_{\text{dip}}$  serves as an input parameter for our calculation. Photon absorption of an equilibrated compound nucleus at excitation energy  $E$  is then governed by the effective absorption rate  $(N\Gamma)_{\text{eff}}(E) = N\Gamma_{\text{dip}} \rho_{\text{acc}}(E)/\rho_{\text{acc}}(E_g)$ . Here  $\rho_{\text{acc}}(E)$  is the density of accessible states and  $E_g$  is the energy of the ground state. The expression for  $(N\Gamma)_{\text{eff}}(E)$  is valid as long as the number  $N_0$  of absorbed photons is small compared to  $N$ . That is the case for the calculations presented below. We equate  $(N\Gamma)_{\text{eff}}(kE_L)$  (the rate for population of the states  $(i, k)$  by dipole absorption of the states  $(i, k-1)$ ) with  $W_{k(k-1)}^2 \rho(i, k)$  in Eq. (1). The stimulated dipole emission width for the inverse transition  $(i, k) \rightarrow (i, k-1)$  is then given by detailed balance as  $(N\Gamma)_{\text{st}}(kE_L) = N\Gamma_{\text{eff}}(kE_L) \rho(i, k-1)/\rho(i, k)$ . In this way, all dipole rates in Eq. (1) are determined. With  $\rho(i, E)$  the level density of nucleus  $(A-i)$  at excitation energy  $E$ , we approximate the density of states  $(i, k)$  as  $\rho(i, k) = \rho(i, kE_L)$ .

The level densities  $\rho(A, E)$  are calculated using the expressions for the total level density of spin-zero states in nucleus  $A$  as a function of excitation energy  $E$  derived in Ref. [9] as functions of the single-particle level density  $\rho_1(\varepsilon)$ . A realistic linear or quadratic energy dependence of  $\rho_1$  is considered,

$$\rho_1^{(1)}(\varepsilon) = \frac{2A}{F^2} \varepsilon, \quad \rho_1^{(2)}(\varepsilon) = \frac{3A}{F^3} \varepsilon^2. \quad (3)$$

Here  $V$  with  $0 \leq \varepsilon \leq V$  defines the range of the single-particle spectrum, and  $F$  is the Fermi energy. The single-particle energies  $\varepsilon_i$  with  $i = 1, 2, \dots$  are obtained from the condition  $i = \int_0^{\varepsilon_i} d\varepsilon' \rho_1(\varepsilon')$ . The expressions (3) are approximately valid for  $A = 100$  and  $A = 200$ , respectively. We have chosen  $V = 45$  MeV and  $F = 37$  MeV and keep these values constant throughout the neutron decay chain. These values also determine the chosen number of total bound single-particle states [9], namely 148 for  $A = 100$  and 360 for  $A = 200$ , respectively.

When the number of nucleons is large, the method [9] fails to work at small excitation energies. In this region we use the Bethe formula [20]. This is done for the first 65 MeV of the excitation energy for the case of medium-weight nuclei ( $A = 100$ ) and the first 200 MeV for heavy nuclei ( $A = 200$ ), i.e., for approximately 10% of the total relevant spectrum. For the density  $\rho_{\text{acc}}(E)$  of accessible states we have used the Fermi-gas model described in Ref. [9] and the same choices of  $\rho_1$  as in Eq. (3).

Figures 2 and 3 give the widths for effective dipole absorption, stimulated dipole emission, neutron emission and the induced fission rates for medium-weight ( $A = 100$ ) and heavy ( $A = 200$ ) nuclei, respectively. Calculation of the latter two rates is explained below. Figures 2 and 3 show that for both medium-weight ( $A = 100$ ) and heavy nuclei ( $A = 200$ ), the effective dipole absorption width  $(NT)_{\text{eff}}(E)$  decreases slowly with increasing excitation energy  $E$ . Over a range of 1000 MeV the decrease amounts typically to a factor of two. The stimulated dipole emission width  $(NT)_{\text{st}}(E)$ , also shown in Figs. 2 and 3, starts out at small excitation energy from a value much below that of  $(NT)_{\text{eff}}(E)$  and increases monotonically with  $E$ . It becomes equal to  $(NT)_{\text{eff}}(E)$  at the maximum  $E_{\text{max}}$  of the level density  $\rho(k)$ . Significant dipole excitation above the energy  $E_{\text{max}}$  is not possible because stimulated emission outweighs here absorption,  $(NT)_{\text{st}}(E) > (NT)_{\text{eff}}(E)$  for  $E > E_{\text{max}}$ . For the two choices of  $\rho_1$  in Eq. (3) we have  $E_{\text{max}} = 533$  MeV and  $E_{\text{max}} = 1200$  MeV, respectively.

We have tacitly assumed that the spreading width  $\Gamma_{\text{sp}}$  retains the value of  $\approx 5$  MeV found at low excitation energy also at the much higher excitation energies relevant for our paper. As is the case for  $(NT)_{\text{eff}}(E)$ , the energy dependence of the spreading width is determined by the relevant density of accessible states. As shown for  $(NT)_{\text{eff}}(E)$  in Figs. 2 and 3, that density changes only moderately with excitation energy. That fact validates our assumption.

## 2. Neutron Decay

For the neutron decay rates we use the Weisskopf estimate

$$\Gamma_N(i, k) = \frac{1}{2\pi\rho(i, k)} \int_0^{(k+1/2)E_L - B_N(i)} dE' \rho(i+1, E'),$$

$$\Gamma_N(i, k \rightarrow k') = \frac{1}{2\pi\rho(i, k)} \int_{(k'-1/2)E_L}^{(k'+1/2)E_L} dE' \rho(i+1, E'). \quad (4)$$

Here  $B_N(i)$  is the neutron binding energy of nucleus  $(A-i)$ . In the second of Eqs. (4) the lower bound is zero for  $k' = 0$ , and  $k'$  is bounded by  $k'E_L \leq kE_L - B_N(i)$ . Eqs. (4) are consistent with Eq. (2). We simplify the calculations by assuming that  $B_N(i) = B_N = 8$  MeV for all  $i = 0, 1, 2, \dots, n$  for the short nuclear chains considered. We thereby neglect the odd-even staggering of binding energies and level densities. These run in parallel and, therefore, largely compensate each other in the neutron decay widths. For both choices for the single-particle level density  $\rho_1$  in Eq. (3), Figs. 2 and 3 show that  $\Gamma_N(k)$

risks steeply with excitation energy. While much smaller than  $(NT)_{\text{eff}}$  for small excitation energies,  $\Gamma_N(k)$  becomes equal to  $(NT)_{\text{eff}}$  at  $E = E_N$  and exceeds  $(NT)_{\text{eff}}$  for  $E > E_N$ . For the two choices of  $\rho_1$  and  $T(E) = 1$  we have  $E_N \approx 435$  MeV and  $E_N \approx 1080$  MeV, respectively. Both values are smaller than the corresponding values of  $E_{\text{max}}$ ,  $E_{\text{max}} = 533$  MeV and  $E_{\text{max}} = 1200$  MeV. We note that the crossing energies  $E_N$  are here larger than the ones presented in Ref. [7], i.e., the neutron rates grow more slowly with excitation energy in the present case. That difference results from our treatment of the Fermi energy  $F$ . In Ref. [7], the Fermi energy changes with mass number  $A$  whereas in the present work, we consider  $F$  fixed. That is in accordance with the fixed value of  $B_N(i) = B_N = V - F = 8$  MeV. The difference  $E_{\text{max}} - E_N$  is sufficiently large in both cases and for both  $A = 100$  and  $A = 200$  to be physically significant, in spite of the inherent uncertainties of the calculation of level densities at high excitation energies. We conclude that neutron evaporation is the limiting factor in nuclear excitation by dipole absorption (provided that fission and proton decay can be neglected).

In Eqs. (4) we have not taken account of the transmission coefficients  $T(E)$ , i.e., the probability of formation of a residual nucleus at excitation energy  $E$  under neutron emission. These obey  $0 \leq T(E) \leq 1$  and should multiply the integrands in Eqs. (4). Neutron decay is dominated by  $s$ -wave neutrons. Here and except for the slowest neutrons the transmission coefficients are of order unity [23]. We test the influence of that approximation (which overestimates the neutron widths) by multiplying all neutron widths by a common factor two. The pairs of dark blue dashed lines in Figs. 2 and 3 show the band of neutron widths for  $T(E)$  in the interval  $1/2 \leq T(E) \leq 1$ . For  $T(E) = 1/2$ ,  $E_N$  is closer to  $E_{\text{max}}$ .

## 3. Fission

According to the Bohr-Wheeler formula [21] modified by friction [22], the maximum width for induced fission (reached at friction constant  $\beta = 0$ ) depends on excitation energy  $E$  essentially as

$$\Gamma_f(i, E) = (\hbar\omega_1/(2\pi)) \exp\{-E_f/T\}. \quad (5)$$

Here,  $E_f$  is the height of the fission barrier,  $\omega_1$  is the frequency of the inverted harmonic oscillator that oscillates the fission barrier at its maximum, and  $T$  is the nuclear temperature. With  $T^{-1} = (d/dE) \ln \rho(i, E)$ , the fission width increases very slowly with  $E$ . That is shown in Figs. 2 and 3 where we present the calculated fission rates for  $\hbar\omega_1 = 4$  MeV and 2 MeV and for  $E_f = 10$  MeV (4 MeV), respectively. The two values of  $E_f$  correspond to  $A = 100$  ( $A = 200$ ), respectively, the fission barrier being lower for heavy nuclei. We see that while perhaps competitive with  $(NT)_{\text{eff}}$  at low excitation energy and for very heavy nuclei, the fission width at higher excitation energy is never competitive with dipole absorption or neutron decay, see Ref. [7]. We must keep in mind, however, that for a sufficiently long laser pulse the processes described by the master equation (1) are ultimately terminated by fission. The induced fission width for  $E = 200$  MeV for a medium-weight nucleus,

for instance, corresponds to a half-life of approximately 5 zs. As shown in the following section by our numerical results, fission is therefore terminating the laser-nucleus reaction after several tens of zs.

Actually, little is known about the dependence of  $\omega_1$  and  $E_f$  on  $E$  for excitation energies in the range of several 100 MeV above yrast. We expect  $E_f$  to decrease with temperature and, more significantly, as ever more neutrons are evaporated. That will speed up the fission process. We have not attempted to estimate the dependence of  $E_f$  on temperature and mass number. Such an estimate would require different techniques and is beyond the scope of this paper.

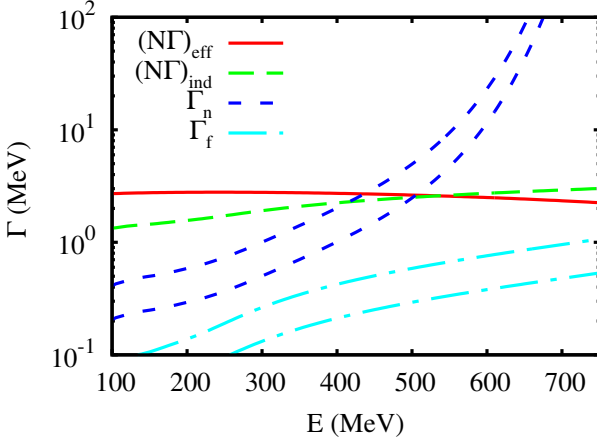


FIG. 2: (color online). Widths for effective dipole absorption (solid red line), stimulated dipole emission (long-dashed green line) (both for  $N\Gamma_{\text{dip}} = 5$  MeV), band for neutron emission (short-dashed dark blue lines) and band for induced fission (dashed-dotted light blue lines) versus excitation energy  $E$  for  $A = 100$  (148 bound single-particle states). The two neutron decay widths are calculated from the Weisskopf estimate ( $T(E) = 1$ ) and by taking for the transmission coefficients uniformly the value  $T(E) = 1/2$ . The two fission widths are obtained using the values  $\hbar\omega_1 = 2$  and 4 MeV.

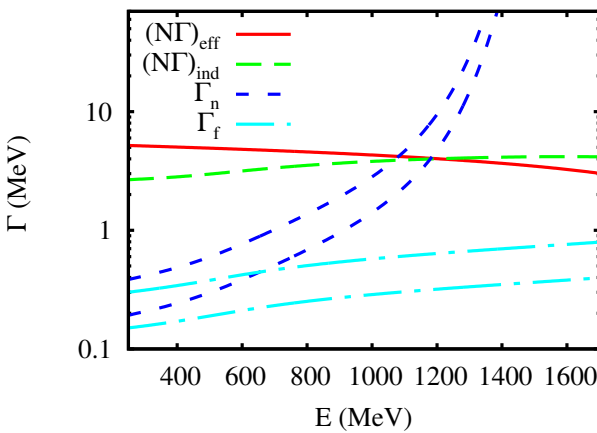


FIG. 3: (color online). Same widths as in Fig. 2 for  $A = 200$  (360 bound single-particle states).

### C. Estimates

Before presenting our numerical results we give some estimates that show roughly what to expect. We estimate the time dependence of the mean excitation energies and the range of nuclei reached by the combination of multiple photon absorption and neutron decay. We recall that the total neutron decay width  $\Gamma_N(E)$  increases steeply with excitation energy  $E$  while the effective dipole absorption width  $(N\Gamma)_{\text{eff}}(E_N)$  decreases slowly with  $E$ . The point  $E_N$  of intersection of the two curves depends on  $(N\Gamma)_{\text{eff}}(E)$  only extremely weakly. For our estimate we therefore use the values  $E_N \approx 435$  MeV and  $E_N \approx 1080$  MeV given in Section III B for all values of  $(N\Gamma)_{\text{eff}}(E)$  and  $\Gamma_N(E)$  considered below. Since the induced fission rates are much smaller than the dipole absorption rate, we neglect fission in this first approximation. Furthermore, we approximate  $(N\Gamma)_{\text{eff}}(E)$  by  $N\Gamma_{\text{dip}}$  for all values of  $E$ . Beyond the critical energy  $E_N$ , neutron evaporation dominates strongly, and it is practically impossible to excite nuclei to energies larger than  $E_N$ . Since  $E_N$  is smaller than the energy  $E_{\text{max}}$  defined by the maximum of the level density, stimulated photon emission is neglected.

Disregarding neutron evaporation we first determine the time and the number of photons needed to reach the energy  $E_N$  in the target nucleus. We approximate the master equation for the target nucleus by the set of equations

$$\dot{P}(0, k, t) = -N\Gamma_{\text{dip}}P(0, k, t) + N\Gamma_{\text{dip}}P(0, k-1, t). \quad (6)$$

The initial condition is  $P(0, k, 0) = \delta_{k0}$ . The solution

$$P(0, k, t) = \frac{(N\Gamma_{\text{dip}}t)^k}{k!} \exp\{-N\Gamma_{\text{dip}}t\} \quad (7)$$

obeys  $\sum_{k=0}^{\infty} P(0, k, t) = 1$  for all times  $t$ . Considering  $P(0, k, t)$  for fixed  $t$  as a function of  $k$  and using Stirling's formula, we find that  $P(0, k, t)$  has a maximum at  $k = k_{\text{max}} = N\Gamma_{\text{dip}}t$  with width  $\sqrt{k_{\text{max}}}$ . The critical energy  $E_N$  with  $k(E_N) = k_N = E_N/E_L$  is reached after absorption of  $N_0 = k_N \pm \sqrt{k_N}$  photons. The time needed for the process is  $t_N = E_N/(E_L N\Gamma_{\text{dip}})$ . For  $A = 100$ ,  $E_N = 435$  MeV,  $E_L = 5$  MeV,  $N\Gamma_{\text{dip}} = 5$  MeV that gives  $N_0 = 87$  photons and  $t_N = 12 \times 10^{-21}$  s. The corresponding figures for  $A = 200$  are  $E_N = 1080$  MeV,  $E_L = 5$  MeV,  $N\Gamma_{\text{dip}} = 5$  MeV,  $N_0 = 216$  photons and  $t_N = 3 \times 10^{-20}$  s. The laser pulse has the required length  $t_N$  in time if  $\sigma \leq 50$  keV or  $\sigma \leq 22$  keV, respectively. The speed of the process increases and the number of absorbed photons decreases as either the photon energy  $E_L$  or the dipole absorption width  $N\Gamma_{\text{dip}}$  or both are increased.

As the process described by Eq. (6) carries on, neutron decay actually depletes  $P(0, k, t)$  and feeds  $P(1, k', t)$ . Even though for energies below  $E_N$  the neutron decay width  $\Gamma_N$  is much smaller than  $N\Gamma_{\text{dip}}$ , the time needed to reach excitation energy  $E_N$  in the target nucleus is sufficiently large that nearly the entire occupation probability in the target nucleus is lost to neutron decay on the way. In the daughter nucleus, photon absorption is described by the same equation (6) save for the feeding term. Neutron decay is dominated by slow neutrons



and, therefore, implies a loss of excitation energy of about 8 MeV (the binding energy). Therefore, feeding of  $P(1, k, t)$  by neutron decay occurs at  $k$  values that are about two units (assuming a photon energy of around 5 MeV) smaller than the ones for which the loss in  $P(0, k, t)$  occurs. It takes about two absorbed photons to make up for that energy loss. The daughter nucleus decays in turn by neutron emission. The process repeats itself in the second daughter nucleus and so on. As a result, the maximum of the occupation probability moves to ever proton-richer nuclei and to ever higher excitation energies, eventually hovering near or at most one or two  $k$  units below  $E_N$ .

An overestimate for the time needed to reach the nucleus with mass number  $(A - i)$  at energy  $E_N$  is obtained by disregarding neutron decay in the target nucleus at energies below  $E_N$ , i.e., by using Eq. (6) up to  $E = E_N$ , and by assuming that at  $E = E_N$  neutron decay takes over and populates the states  $(1, k_N - 2)$  in the nucleus  $(A - 1)$  (this scenario is consistent with  $E_L = 5$  MeV). These are dipole-excited twice till the next neutron decay sets in, and so on. Since at  $E = E_N$  we have  $\Gamma_N(E_N) = N\Gamma_{\text{dip}}(E_N)$ , the part of the master equation describing the feeding of the first daughter nucleus by neutron decay of the target nucleus reads

$$\begin{aligned} \dot{P}(1, k_N - 2, t) = & -N\Gamma_{\text{dip}}P(1, k_N - 2, t) \\ & + N\Gamma_{\text{dip}}P(0, k_N, t). \end{aligned} \quad (8)$$

The loss term accounts for photon absorption in nucleus  $(A - 1)$ . From here Eq. (6) with  $i = 0$  replaced by  $i = 1$  takes over until the energy  $E_N$  is reached in nucleus  $(A - 1)$ . That is the case after absorption of two photons. The process continues, alternating between Eq. (6) and the analogue of Eq. (8) for the second, third,  $\dots$ , daughter nucleus. Except for the counting of  $k$  values, these combined equations all have the same form as Eq. (6), and their solution, therefore, has the form of the right-hand side of Eq. (7). Hence

$$P(i, k_n, t) = \frac{(N\Gamma_{\text{dip}}t)^{k_n+3i}}{(k_n+3i)!} \exp\{-N\Gamma_{\text{dip}}t\}. \quad (9)$$

The function  $P(i, k_n, t)$  has its maximum at  $t = (k_n + 3i)/(N\Gamma_{\text{dip}})$ . In other words, while it takes 87 (216) photons to reach  $E_N$  from the ground state of the target nucleus with mass number  $A = 100$  ( $A = 200$ , respectively), it takes only 15 additional absorbed photons to move 5 mass units away from the line of stability. The additional time needed is  $15/(N\Gamma_{\text{dip}})$ . These figures show that once the threshold energy  $E_N$  for significant neutron evaporation is reached, the process quickly populates nuclei far from the valley of stability. The spread  $\sigma$  of the laser pulse needed to reach the energy  $E_N$  is given by

$$\sigma_0 = N\Gamma_{\text{dip}}E_L/E_N. \quad (10)$$

Here  $E_N$  is independent of  $E_L$ . With  $E_N = 435$  MeV and  $E_N = 1080$  MeV for mass numbers  $A = 100$  and  $A = 200$ , respectively, Eq. (10) defines a relation between the experimental parameters  $\sigma$ ,  $E_L$ , and  $N\Gamma_{\text{dip}}$ . The formation of proton-rich nuclei sets in whenever  $\sigma \leq \sigma_0$ . Clearly, these times are overestimates because neutron decay is actually simultaneous with

(and not subsequent to) photon absorption. After several tens, fission puts an end to the process, sooner for heavy nuclei than for medium-weight ones.

#### IV. NUMERICAL RESULTS

We calculate the time-dependent occupation probabilities  $P(i, k, t)$  for medium-weight ( $A = 100$ ) and heavy ( $A = 200$ ) target nuclei that interact with a short pulse of coherent MeV photons. We solve Eq. (1) numerically for several choices of photon energy  $E_L$ , of the effective dipole width  $N\Gamma_{\text{dip}}$ , and of the length  $(n+1)$  of the decay chain. Eq. (1) is written in matrix form (including target and daughter index  $i = 0, 1, \dots, n$ ) as  $\dot{\mathcal{P}} = \mathcal{M}\mathcal{P}$  with  $P(i, k, t) \rightarrow \mathcal{P}(k + i(k_{\text{max}} + 1), t)$  and  $k_{\text{max}}$  the maximum number of excitation steps considered. The matrix  $\mathcal{M}$  is independent of time and has both block-diagonal parts (fixed index  $i$ ) describing dipole absorption, stimulated emission, neutron decay and fission, as well as non-diagonal feeding terms for the daughter nuclei [mass  $(A - i)$ ] which are populated by neutron decay of their predecessors [mass  $(A - i + 1)$ ]. The formal solution of Eq. (1) in vector form is  $\mathcal{P}(t) = \exp\{\mathcal{M}t\}\mathcal{P}(t = 0)$ . Because of the strongly varying rates and the large level densities involved (for instance,  $\rho(E_{\text{max}}) \simeq 10^{104} \text{ MeV}^{-1}$  for  $A = 200$ ), severe numerical problems may arise when one attempts to use standard linear algebra routines such as LAPACK [24] for the calculation of the matrix exponential.

Dedicated matrix exponential methods for solving systems of extremely stiff differential equations, i.e., equations for which the solving methods are numerically unstable, unless the step size is taken to be extremely small, have been developed in the last half-century [25–27] and applied, e.g., to nuclear fuel burnup calculations [28–30]. In this work, we employ a new fast general-purpose semi-analytical matrix exponential solver, which is based on a combination of backward-stable matrix algorithms [31]. To verify numerical accuracy, we additionally carry out comparative calculations with other state-of-the-art solvers for the particularly demanding case of heavy nuclei with  $A = 200$ .

Fig. 4 shows the target occupation probability  $P(0, E, t) = P(0, kE_L, t)$  in the absence of both neutron decay and fission for photon energy  $E_L = 5$  MeV and for  $A = 100$  and  $N\Gamma_{\text{dip}} = 1, 5, 8$  MeV. Depending on the effective dipole width, the saturation energy  $E_{\text{max}} = 533$  MeV where stimulated emission limits photon absorption is reached after 50 zs for  $N\Gamma_{\text{dip}} = 8$  MeV (after 100 zs for  $N\Gamma_{\text{dip}} = 5$  MeV, respectively). The energy  $E_N$  above which  $\Gamma_N > (N\Gamma)_{\text{eff}}$  is reached for the case of  $N\Gamma_{\text{dip}} = 5$  MeV much later than the time estimated in Sec. III C of  $t_N = 12$  zs. A neck-like artifact can be observed at the switching point  $E = 68$  MeV in the calculation method for the level densities  $\rho(i, k)$  and is best visible in Fig. 4a. Additional information is provided by value and position of the maximum and by the FWHM of the occupation probability shown in the lower part of the figure for the three cases considered. In accord with our estimates in Sec. III C the FWHM is proportional to  $\sqrt{t}$  and, after the first few zs, the peak height has a  $1/\sqrt{t}$  dependence. The linear dependence

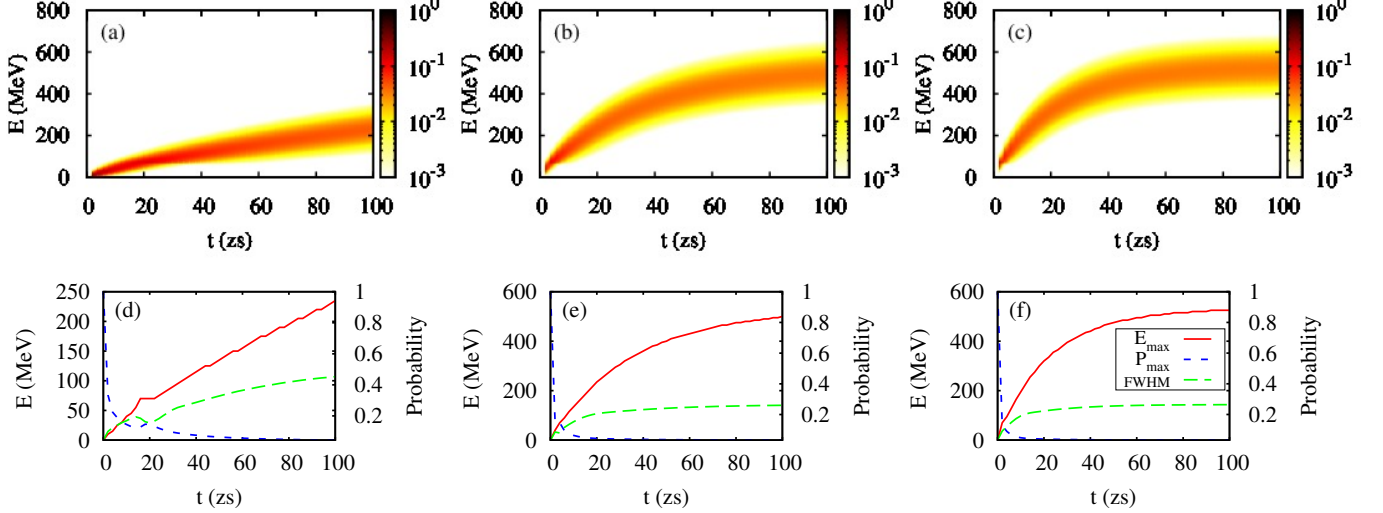


FIG. 4: (color online). Occupation probabilities  $P(0, E, t)$  for  $E_L = 5$  MeV,  $A = 100$  and for dipole absorption and stimulated emission only. (a-c) Contour plots of the time-dependent occupation probability  $P(0, E, t)$  as a function of excitation energy  $E$  for (a)  $NT_{\text{dip}} = 1$  MeV, (b)  $NT_{\text{dip}} = 5$  MeV and (c)  $NT_{\text{dip}} = 8$  MeV. (d-f) Corresponding peak height (dashed blue line) (scale on the right  $y$ -axis), position (solid red line), and FWHM (long-dashed green line) of the occupation probability (scales on the left  $y$ -axis) for (d)  $NT_{\text{dip}} = 1$  MeV, (e)  $NT_{\text{dip}} = 5$  MeV and (f)  $NT_{\text{dip}} = 8$  MeV.

of the maximum on time holds only for the smallest of the three values of  $NT_{\text{dip}}$  and does so only for small times. In all other cases stimulated dipole emission slows down the linear increase. The switching point at  $E = 68$  MeV is also visible here in the shape of kinks in the three curves illustrating the peak position, height and FWHM of the occupation probability in Fig. 4d.

Fig. 5 shows qualitatively similar results for a target nucleus with  $A = 200$ . The time dependence of the peak position, maximum peak value and FWHM again confirm our estimates in Sec. III C, except that the linear approximation for the peak position is only valid for short times  $t$  (except for the case  $NT_{\text{dip}} = 1$  MeV). Reaching the saturation energy  $E_{\text{max}} = 1200$  MeV requires a substantially larger number of absorbed photons than for  $A = 100$ . The switching point between the calculation methods for the level densities  $\rho(i, k)$  at  $E = 200$  MeV is also here visible, especially in Figs. 5a and 5d.

Laser excitation of heavy nuclei ( $A = 200$ ) poses a numerically challenging problem, due to increased stiffness of the equation system. We have used the parameter set  $A = 200$ ,  $E_L = 5$  MeV,  $NT_{\text{dip}} = 5$  MeV, as testing ground for five state-of-the-art equation solvers that employ matrix exponential methods: (1) the semi-analytical matrix exponential method [31], (2) the Chebyshev Rational Approximation Method (CRAM) with partial fraction coefficients for approximation order 14 [29, 32], (3) CRAM with partial fraction coefficients for approximation order 16 [29, 32], (4) eigenvector decomposition of matrix  $\mathcal{M}$  and (5) a modern scaling and squaring Taylor expansion algorithm [33]. The five solvers were used to reproduce Fig. 5b. The comparison shows that differently calculated  $P(0, E, t)$  values agree within an accuracy of  $10^{-3}$ . All methods produce some numerical artifact in the

form of fringes on the upper side of  $P(0, k, t)$  on an accuracy level of  $10^{-4} - 10^{-5}$ . We do not expect that such a level of accuracy can be attained in experiments in the foreseeable future and consider these fringes irrelevant. The semi-analytical algorithm used in the present work [31] is the fastest one, yielding results in less than a minute, while the slowest scaling and squaring Taylor expansion method required more than two weeks for the same parameter set.

While Fig. 4 shows how the value of  $NT_{\text{dip}}$  affects the speed of nuclear excitation, Fig. 6 displays the influence of  $E_L$ . We take  $E_L = 1, 5$  and  $10$  MeV and use the same dipole absorption width  $NT_{\text{dip}} = 5$  MeV throughout. The dependence of the occupation probability  $P(0, E, t)$  on photon energy  $E_L$  is shown in Fig. 6 for the generic medium-weight target nucleus with  $A = 100$  and in the absence of neutron decay. Depending on photon energy, the saturation region is reached after 400, 100 or 50 zs, respectively. A large photon energy speeds up the excitation process and may partially counteract the effect of a small dipole absorption width  $NT_{\text{dip}}$ . For  $E_L = 1$  MeV the excitation path is energetically more narrow than in the other cases. In summary, photon energy  $E_L$  and dipole absorption width  $NT_{\text{dip}}$ , (i.e., the number of coherent photons in the laser pulse) jointly determine the time scale of the excitation process. We add few technical remarks: Due to the smaller excitation energy per step of the calculation, the case  $E_L = 1$  MeV is more sensitive to where we switch from the Bethe formula to our method for the calculation of nuclear level densities. That point shows up as a small neck at  $\approx 68$  MeV excitation energy in all three plots in Fig. 6. In addition, the numerical effort for  $E_L = 1$  MeV is much larger than for higher values of  $E_L$  as it requires both a large matrix and, because of the slower excitation process, many more time points. The difference in the



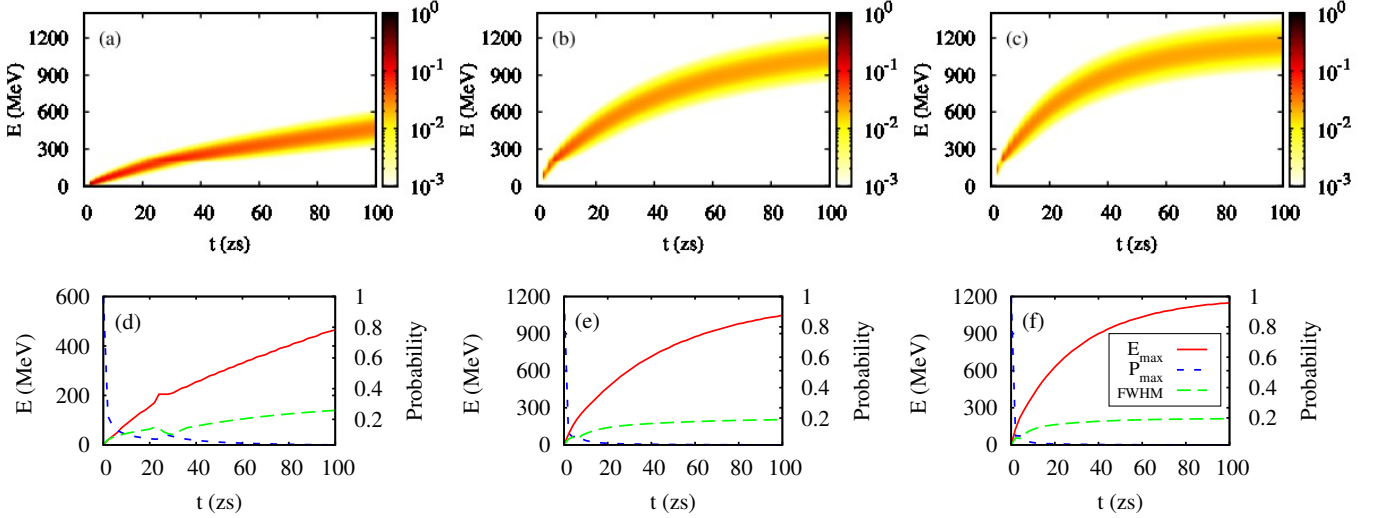


FIG. 5: (color online). Occupation probabilities  $P(0, E, t)$  for  $E_L = 5$  MeV,  $A = 200$  and for dipole absorption and stimulated emission only. (a-c) Contour plots of the time-dependent occupation probability  $P(0, E, t)$  as a function of excitation energy  $E$  for (a)  $NT_{\text{dip}} = 1$  MeV, (b)  $NT_{\text{dip}} = 5$  MeV and (c)  $NT_{\text{dip}} = 8$  MeV. (d-f) Corresponding peak height (dashed blue line) (scale on the right  $y$ -axis), position (solid red line), and FWHM (long-dashed green line) (scales on the left  $y$ -axis) of the occupation probability and for (d)  $NT_{\text{dip}} = 1$  MeV, (e)  $NT_{\text{dip}} = 5$  MeV and (f)  $NT_{\text{dip}} = 8$  MeV.

energy spacing also affects the contour plots, creating the false impression that the integral over occupation probability at any one time is smaller for small  $E_L$ . Numerically, for any time  $t$  the sum over all occupation probabilities  $\sum_k P(0, k, t)$  equals unity with accuracy better than  $10^{-6}$  for all three considered photon energies  $E_L$ .

We now take account of neutron decay of the target and of three consecutive daughter nuclei, still neglecting fission. We solve the master equation for a chain of five nuclei with mass numbers ranging from  $A$  to  $A - 4$ . We disregard neutron emission by the last nucleus with mass number  $A - 4$  which serves as a dump for the overall probability flow. The dimensions of the matrices  $\mathcal{M}$  are five times larger than for the parent nucleus only. In particular, for photon energy  $E_L = 5$  MeV the matrix dimension is 500 (1000) for an  $A = 100$  (an  $A = 200$ ) target nucleus, respectively. Fig. 7 shows contour plots of the occupation probabilities  $P(i, E, t)$  for  $i = 0$  (target) and  $i = 1, 2, 3, 4$  (daughters) and for three parameter sets as indicated. In all cases, the final nucleus in the chain undergoes only dipole excitation with energies eventually reaching the saturation energy. Compared to pure dipole absorption, neutron emission is seen to broaden the distribution, cf. Figs. 4b and 5b. The occupation probabilities  $P(i, E, t)$  with  $i \leq 3$  show that neutron emission comes into play early, slowing down the excitation process even at energies below  $E_N$ , i.e., below  $\approx 435$  MeV for  $A = 100$  and 1080 MeV for  $A = 200$ , respectively. As soon as the neutron emission rates reach approximately  $10^{20} \text{ s}^{-1}$ , sufficiently many daughter nuclei are produced within the tens of zs time span of the laser pulse to strongly deplete the occupation probability of the target nucleus. A comparison of the probability distributions of  $A = 100$  parent nuclei for photon energies  $E_L$  of 5 and 10 MeV energy (columns (i) and (ii) in

Fig. 7) shows that higher excitation energies are reached (and correspondingly stronger neutron decay sets in) as the photon energy is increased. For  $t = 10$  zs and for  $E_L = 10$  MeV most of the nuclei have disintegrated to the dump ( $i = 4$ ), while for  $E_L = 5$  keV the target nucleus and the first daughter  $i = 0, 1, 2$  are still predominantly occupied at  $t < 10$  zs. Comparing columns (i) and (iii) of Fig. 7 we note that for identical times  $t$ , higher excitation energies are reached in the heavier target. That is possible because of the much higher value of  $E_N = 1080$  MeV for  $A = 200$ . As is the case for  $A = 100$ , neutron emission plays an important role long before the excitation energy  $E_N$  is reached. After 10 zs, the occupation probability of the target nucleus practically vanishes, while the occupation probabilities for nuclei with  $i = 2, 3$  and even  $i = 4$  are significant.

Fission is taken into account by adding the fission width as a diagonal loss term in Eq. (1). We do not follow the fate of the fission products as their masses are much smaller than those of the target nucleus and of the first few daughter nuclei. For a one-to-one comparison, results are shown in Fig. 8 for the same set of parameters as used in Fig. 7. As expected from the decay rates shown in Sec. III B, Fig. 8 shows that neutron emission is much faster than fission. For  $A = 100$ , fission is so much slower than neutron decay that the comparison of the results for the target (T) and the first three daughter (D1-D3) nuclei shows little difference between the cases without and with fission. Only for the last nucleus in the chain, where neutron decay is switched off, we do reach the time scale for which the fission rate produces significant loss. Since heavy nuclei ( $A = 200$ ) have a larger fission width, some loss of probability can be observed already for the first daughter nucleus and for the daughters with  $i = 3$  and  $i = 4$  the occupation probabilities

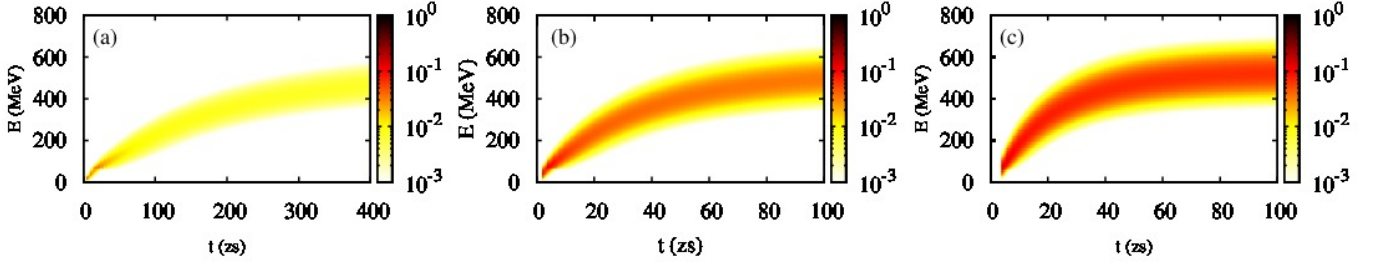


FIG. 6: (color online). Contour plots of the time-dependent occupation probability  $P(0, E, t)$  as a function of excitation energy  $E$  for (a)  $E_L = 1$  MeV, (b)  $E_L = 5$  MeV and (c)  $E_L = 10$  MeV. The results are for  $N\Gamma_{\text{dip}} = 5$  MeV,  $A = 100$ , and for dipole absorption and stimulated emission only.

almost vanish. The effective loss of total occupation probability  $\sum_{i,k} P(i, k, t) = 0$  is displayed in Fig. 9 for all three cases (i), (ii) and (iii).

## V. DISCUSSION

The results of Section IV are obtained under neglect of the direct emission of nucleons by photoabsorption into the continuum. As shown in Ref. [7], such direct emission plays only a minor role for nuclei around  $A = 100$  but is competitive with neutron decay for heavy nuclei. The effective charges of neutrons and protons being nearly equal in magnitude, such direct photoionization is expected to produce neutrons and protons in about equal numbers. As a consequence, photoabsorption populates highly excited states not only in the chain of nuclei reached by neutron emission, but also in all nuclei with mass numbers  $(A - i)$  that lie between the valley of stability and nuclei in that chain. We have not attempted to calculate that process in detail.

Fission ultimately terminates all the processes considered in this paper. Characteristic time scales are given in Fig. 9. The study of nuclei at high excitation energies and far off the line of stability is possible only when the laser pulse terminates before that characteristic time, i.e., if  $\sigma \geq \Gamma_f$ . It was mentioned above that we expect  $\Gamma_f$  to increase with increasing distance of the fissioning nuclei from the valley of stability. A reliable estimate would require a precise calculation of the height of the fission barrier  $E_f$  versus that distance. Termination by fission of the processes considered in this paper would allow to measure  $\Gamma_f$  and, thus, to check such calculations.

It was pointed out by A. Richter [34] that at excitation energies of several 100 MeV, the compound nucleus might undergo transitions in which excited states of the nucleon are populated or in which subthreshold pion production occurs. How likely are such processes (which we have disregarded in this paper)? In the quasiadiabatic regime, the compound nucleus is near equilibrium at all times, and the answer follows from a statistical argument. The large number of equilibrium con-

figurations at energy  $E$  must be compared with the very much smaller number of configurations where (almost) all the energy resides in a single mode (that of the excited nucleon or that of the pion). The situation is comparable to the emission of a fast neutron that carries almost all the excitation energy of the compound nucleus and leaves the residual nucleus in a state of low excitation energy. In comparison with slow-neutron emission, this process is suppressed by up to twenty orders of magnitude. We expect a large suppression factor also for the processes under discussion. However, each of these processes is easily distinguishable experimentally from any of the processes considered in our paper. In spite of their enormous scarcity, formation of any of the  $\Delta$  resonances or subthreshold pion production might, therefore, still be observable.

## Appendix A:

We calculate the distribution of spin values in the target nucleus after absorption of  $N_0$  photons. We take the direction of propagation of the photons as  $z$ -axis. In an unpolarized laser beam each dipole photon carries angular momentum  $z$ -component  $\pm 1$ . Absorption of a single photon populates nuclear states with  $J_z = \pm 1$ . These correspond to total spin  $J = 1$ . Absorption of two photons populates nuclear states with  $J_z = \pm 2$  (once each) and  $J_z = 0$  (twice), corresponding to  $J = 2$  (once) and  $J = 0$  (once). Absorption of  $N_0$  photons populates states with  $J_z = \pm N_0, \pm N_0 \mp 2, \pm N_0 \mp 4, \dots$ . Inspection shows that the multiplicity of states with given  $|J_z|$  is given by  $\binom{N_0}{k}$  where  $2k = |J_z| + N_0$  and  $k = N_0/2, N_0/2 + 1, \dots, N_0$  for  $N_0$  even and  $k = (N_0 + 1)/2, (N_0 + 3)/2, \dots, N_0$  for  $N_0$  odd. We note that for  $N_0$  even (odd) only even (odd) values of  $J_z$  and, thus, of total spin  $J$  occur. The number  $Z(J)$  of such spin values is given by  $\binom{N_0}{k} - \binom{N_0}{k+1}$  with  $2k = J + N_0$ . For  $N_0 \gg 1$  we use Stirling's formula and approximate the difference by the negative derivative with respect to  $k$ . Thus,

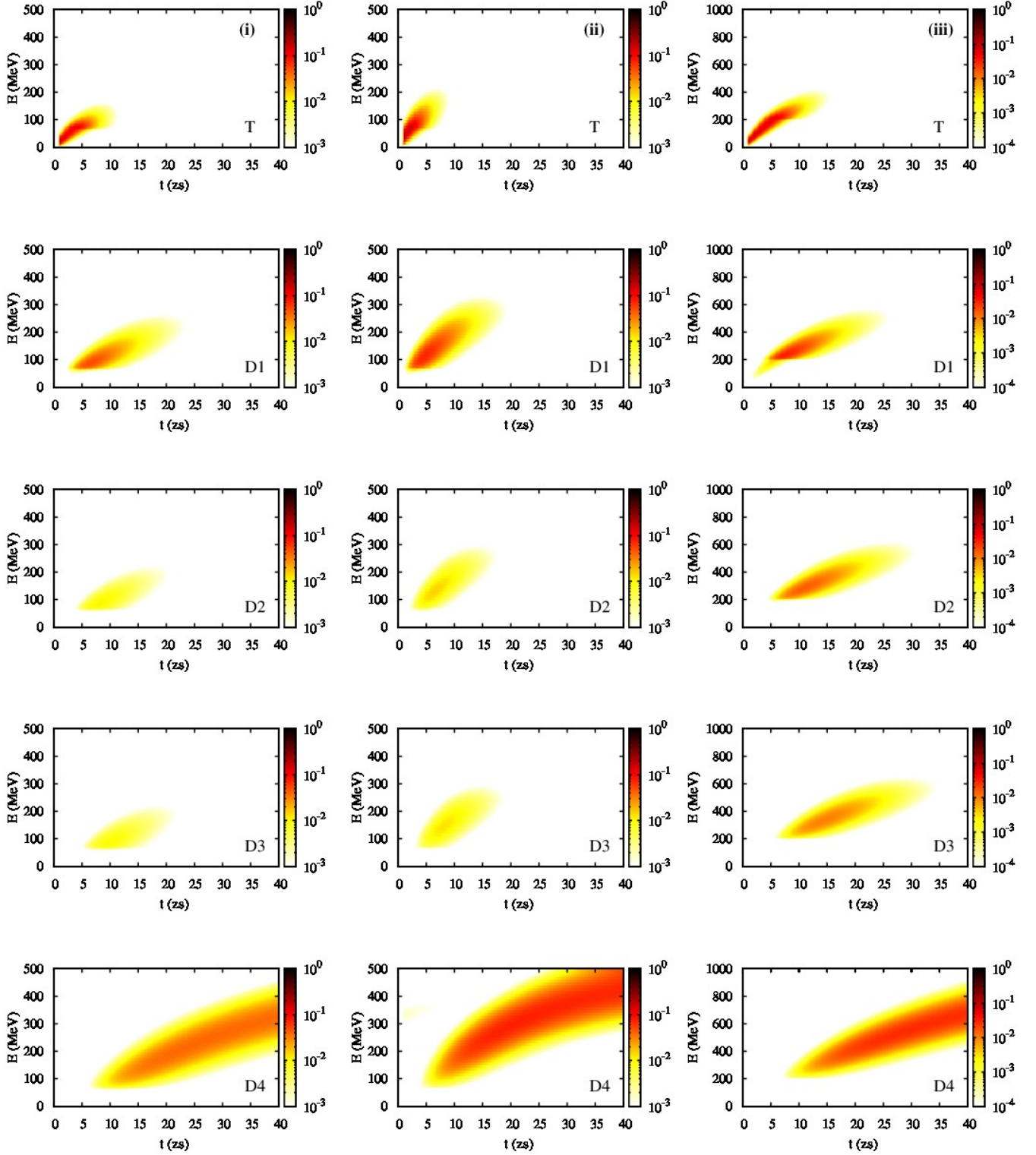


FIG. 7: (color online). Contour plots of the time-dependent occupation probabilities  $P(i, E, t)$  with (from top to bottom) target nucleus ( $i = 0$ , label  $T$ ) and four daughter nuclei ( $i = 1$  to  $4$ , labels  $D1 - D4$ ) as functions of excitation energy  $E$  for  $NT_{\text{dip}} = 5$  MeV. Left column: Target nucleus  $A = 100$ , photon energy  $E_L = 5$  MeV; middle column: Target nucleus  $A = 100$ , photon energy  $E_L = 10$  MeV; right column: Target nucleus  $A = 200$ , photon energy  $E_L = 5$  MeV. Please note the different color coding span for the case with target nucleus  $A = 200$ , which we chose for purpose of comparison with the next figure.

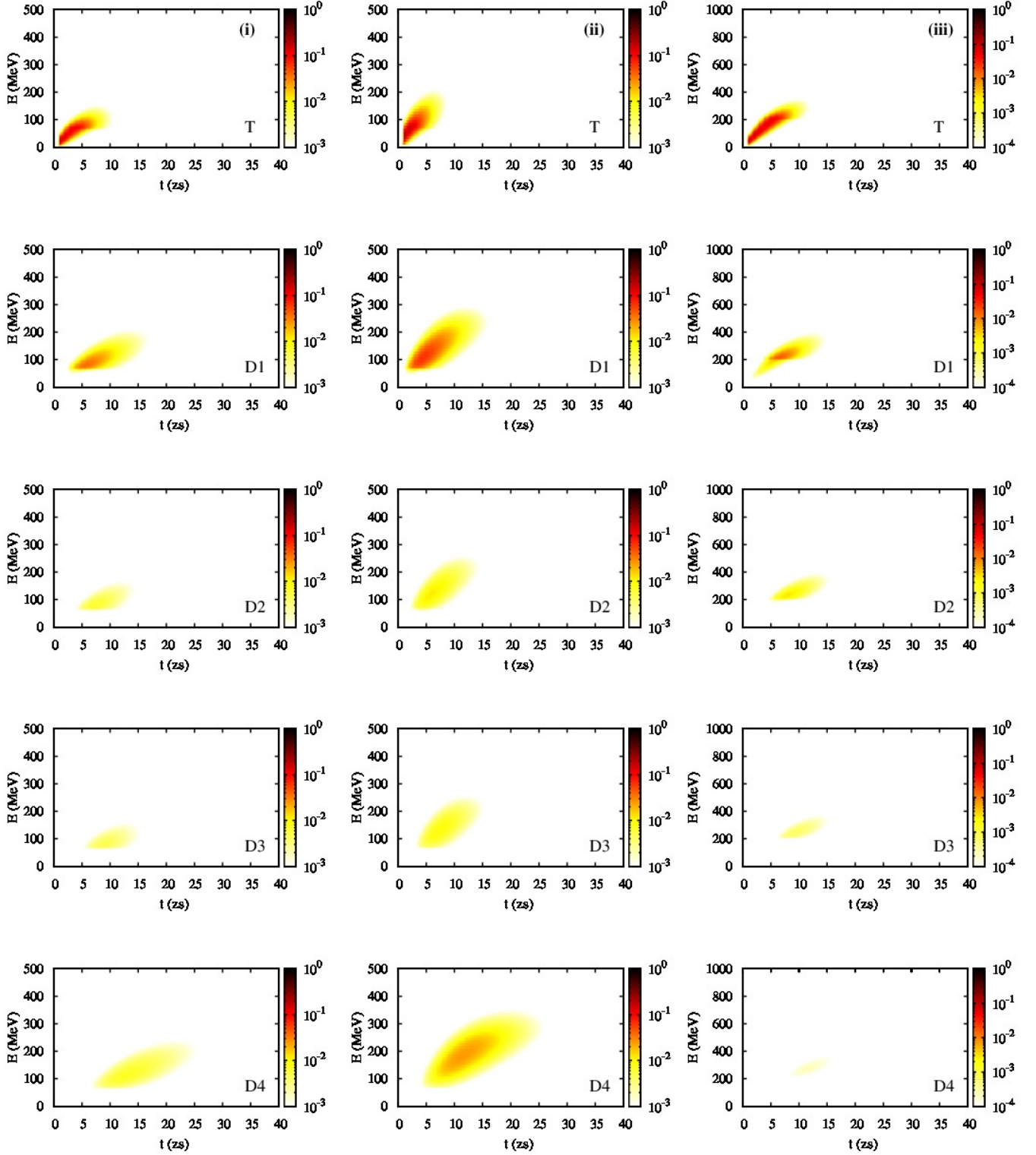


FIG. 8: (color online). Same as Fig. 7 but including induced fission.

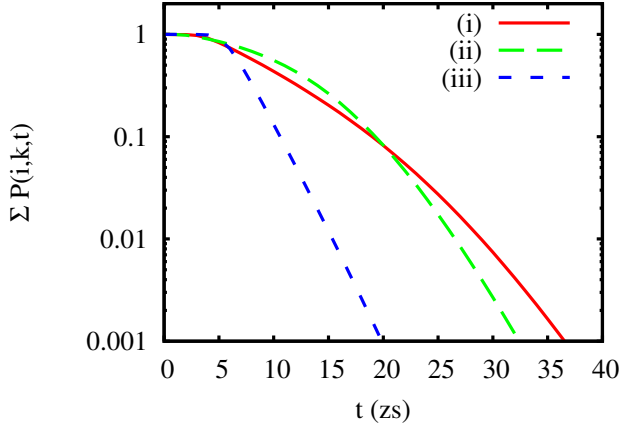


FIG. 9: (color online) Loss of total occupation probability  $\sum_{i,k} P(i,k,t)$  due to fission for the three parameter sets used in Figs. 7 and 8:  $NT_{\text{dip}} = 5$  MeV in all cases, (i) target nucleus with  $A = 100$ , photon energy  $E_L = 5$  MeV (solid red line), (ii) target nucleus with  $A = 100$ , photon energy  $E_L = 10$  MeV (long-dashed green line), and (iii) target nucleus with  $A = 200$ , photon energy  $E_L = 5$  MeV (short-dashed blue line).

$$Z(J) = -\frac{d}{dk} \left( \frac{N_0}{k} \right) \Big|_{k=(N_0+J)/2} \approx \ln \frac{N_0 - J}{N_0 + J} \exp \{ N_0 \ln N_0 - (1/2)(N_0 + J) \ln(N_0 + J)/2 - (1/2)(N_0 - J) \ln(N_0 - J)/2 \}. \quad (\text{A1})$$

By definition,  $Z(J) \geq 0$ . We note that  $Z(J) = 0$  at  $J = 0$ . Inspection shows that  $Z(J)$  has a single maximum and drops off to relatively small values for  $J \approx N_0$ . The maximum  $J_0$  of

$Z(J)$  is located at  $J_0 = \sqrt{N_0}$ . We have used  $J_0 \ll N_0$ . For  $N_0 \gg 1$  that condition is met by the solution (A1).

- 
- [1] G. Mourou and T. Tajima, *Science* **331**, 41 (2011).
  - [2] Extreme Light Infrastructure, URL: [www.extreme-light-infrastructure.eu](http://www.extreme-light-infrastructure.eu), (2015).
  - [3] International Center on Zetta-Exawatt Science and Technology, URL: [www.izest.polytechnique.edu](http://www.izest.polytechnique.edu) (2015).
  - [4] K. Krajewska, M. Twardy, and J. Z. Kamiński, *Phys. Rev. A* **89** (2014) 052123, K. Krajewska and J. Z. Kamiński, preprint arXiv:1410.1026 (2014).
  - [5] A. Di Piazza, C. Müller, K. Z. Hatsagortsyan, and C. H. Keitel, *Rev. Mod. Phys.* **84**, 1177 (2012).
  - [6] H. A. Weidenmüller, *Phys. Rev. Lett.* **106**, 122502 (2011).
  - [7] A. Pálffy and H. A. Weidenmüller, *Phys. Rev. Lett.* **112**, 192502 (2014).
  - [8] A. Pálffy and H. A. Weidenmüller, *Phys. Lett. B* **718**, 1105 (2013).
  - [9] A. Pálffy and H. A. Weidenmüller, *Nucl. Phys. A* **917**, 15 (2013).
  - [10] L. V. Keldysh, *Sov. Phys. JETP* **20**, 1307 (1965).
  - [11] A. Pálffy, J. Evers, and C. H. Keitel, *Phys. Rev. C* **77**, 044602 (2008).
  - [12] H. A. Weidenmüller and G. E. Mitchell, *Rev. Mod. Phys.* **81**, 539 (2009).
  - [13] B. Dietz and H. A. Weidenmüller, *Phys. Lett. B* **693**, 316 (2010).
  - [14] G. E. Mitchell, A. Richter and H. A. Weidenmüller, *Rev. Mod. Phys.* **82**, 2845 (2010).
  - [15] D. B. Milosevic, G. G. Paulus, D. Bauer, and W. Becker, *J. Phys. B: At. Mol. Opt. Phys.* **39**, R203 (2006).
  - [16] S. V. Popruzhenko, *J. Phys. B: At. Mol. Opt. Phys.* **47**, 204001 (2014).
  - [17] H. A. Weidenmüller, *AIP Conf. Proc.* **1005**, 151 (2008).
  - [18] C. A. Bertulani, arXiv:0908.4307v1 [nucl.th].
  - [19] O. Benhar, D. Day, and I. Sick, *Rev. Mod. Phys.* **80**, 189 (2008).
  - [20] H. A. Bethe, *Phys. Rev.* **50**, 332 (1936).
  - [21] N. Bohr and J. A. Wheeler, *Phys. Rev.* **56**, 426 (1939).
  - [22] P. Grange, J. Q. Li, and H. A. Weidenmüller, *Phys. Rev. C* **27**, 2063 (1983).
  - [23] E. H. Auerbach and F. G. J. Perey, *Optical Model Neutron Transmission Coefficients, 0.1 to 5.0 MeV*, vol. 765 of BNL series, Brookhaven National Laboratory (1962).
  - [24] E. Anderson, Z. Bai, C. Bischof, L. S. Blackford, J. Demmel, J. Dongarra, J. du Croz, A. Greenbaum, S. Hammarling, A. McKenney, and D. Sorensen, *LAPACK Users' Guide*, (Society for Industrial and Applied Mathematics SIAM, Philadelphia, PA, 1999).
  - [25] W. J. Cody, G. Meinardus and R. S. Varga, *J. Approx. Theory* **2**,

- 50 (1969).
- [26] E. Hairer and G. Wanner, *Solving Ordinary Differential Equations. Stiff and Differential-Algebraic Problems*, Springer Series in Computational Mathematics vol. 14, 2nd Edition, Springer, 1996.
  - [27] C. Moler and C. van Loan, SIAM Rev. **45**, 3 (2003).
  - [28] M. Pusa and J. Leppänen, Nucl. Sci. Eng. **164**, 140 (2010).
  - [29] M. Pusa, Nucl. Sci. Eng. **169**, 155 (2011).
  - [30] A. Stankovskiy, G. Van den Eynde, Sci. Technol. Nucl. Ins. **2012**, 545103 (2012).
  - [31] A. Hoefer and O. Buss, in preparation (2015).
  - [32] M. Pusa, arXiv:1206.2880 (2012).
  - [33] A. H. Al-Mohy and N. J. Higham, Siam J. Sci. Comput. **33**, 488 (2011).
  - [34] A. Richter, private communication (2014).